Clinical Neurophysiology 123 (2012) 1676–1686

Contents lists available at SciVerse ScienceDirect

Clinical Neurophysiology

journal homepage: www.elsevier.com/locate/clinph

Muscle artifacts in multichannel EEG: Characteristics and reduction

Junshui Ma [a,*], Peining Tao [b], Sevinç Bayram [c], Vladimir Svetnik [a]

[a] Biometrics Research, Merck Research Laboratories, Merck & Co. Inc., Rahway, NJ, USA
[b] Wellinfo Consulting, LLC, Edison, NJ, USA
[c] Polytechnic Institute of New York University, New York, NY, USA

See Editorial, pages 1481–1482

ARTICLE INFO

Article history:
Available online 11 January 2012

Keywords:
Electroencephalography (EEG)
Muscle artifacts
Independent Component Analysis (ICA)
Muscle signal characteristics
Clinical EEG
Clinical trial
Pharmaco-EEG
Drug effect
Muscle signals
Muscle characteristics

HIGHLIGHTS

- This study expands our knowledge of muscle activities in EEG from muscle-controlled experiments to general clinical trials by studying the temporal, spectral, and spatial signal characteristics of unintentional muscle activities.
- The proposed high-throughput muscle artifact reduction method provides an urgently needed solution with validated performance for processing large volumes of clinical EEG.
- The muscle activity topography generated by the proposed method can be used as a biofeedback tool to reveal the unintentionally stressful spots on a person's head.

ABSTRACT

Objective: To study the characteristics of unintentional muscle activities in clinical EEG, and to develop a high-throughput method to reduce them for better revealing drug or biological effects on EEG.
Methods: Two clinical EEG datasets are involved. Pure muscle signals are extracted from EEG using Independent Component Analysis (ICA) for studying their characteristics. A high-throughput method called ICA-SR is introduced based on a new feature named Spectral Ratio (SR).
Results: The spectral and temporal characteristics of the muscle artifacts are illustrated using representative muscle signals. The spatial characteristics are presented at both the group- and the subject-level, and are consistent under three different electrode reference methodologies. Objectively compared with an existing method, ICA-SR is shown to reduce more artifacts, while introduce less distortion to EEG. Its effectiveness is further demonstrated in real clinical EEG with the help of a CO_2-inhalation EEG recording session.
Conclusion: The characteristics of unintentional muscle activities align with the reported characteristics of controlled muscle activities. Artifact spatial characteristics can be EEG equipment dependent. The ICA-SR method can effectively and efficiently process clinical EEG.
Significance: Armed with advanced signal processing algorithms, this study expands our knowledge of muscle activities in EEG from muscle-controlled experiments to general clinical trials. The ICA-SR method provides an urgently needed solution with validated performance for efficiently processing large volumes of clinical EEG.

1. Introduction

It is a well-recognized problem that electroencephalography (EEG) signals are frequently contaminated by skeletal and facial muscle activities, i.e. muscle artifacts (Barlow, 1986; Goncharova et al., 2003; Fatourechi et al., 2007). Muscle artifacts add an excessive amount of high-frequency signal components to normal EEG signals in the time domain, and overwhelm the EEG power spectra at the Beta and Gamma bands in the frequency domain (Goncharova et al., 2003; Fatourechi et al., 2007). Their uncontrollable nature increases EEG variability, and thus reduces EEG's power to detect the functional states of the brain, to evaluate drug effects, and to diagnose psychiatric and neurological disorders.

* Corresponding author. Address: Biometrics Research, Merck Research Laboratories, Merck & Co. Inc., RY33-300, 126 E Lincoln Ave., Rahway, NJ 07065-0900, USA. Tel.: +1 732 594 6941; fax: +1 732 594 1565.
E-mail address: junshui_ma@merck.com (J. Ma).

1388-2457/$36.00
doi:10.1016/j.clinph.2011.11.083

Compared with other well-studied EEG artifacts, e.g. ocular artifacts, there are very few efforts devoted to muscle artifacts, which is surprising considering their ubiquity. Practical and efficient artifact reduction solutions are even sparser. One of the possible reasons is that EEG at the high frequent range was not systematically studied because a typical sampling rate was no more than 100 Hz until the recent decades. Among the 250 papers surveyed by Fatourechi et al. (2007), about 80% of them either ignored the issue of muscle artifacts, or left the artifacts untreated. Also, only 3.2% of them used an automatic method to remove/reduce the muscle artifacts. This situation is primarily due to the lack of (a) a good understanding of the complex nature of muscle artifacts and (b) an easy access to validated artifact reduction methods and software packages.

This study attempts to address both issues. We first study the characteristics of unintentional muscle activities using a data-driven approach. Based upon our acquired knowledge of the muscle activities, a muscle reduction method suitable for continuous clinical EEG is proposed, and validated.

Goncharova et al. (2003) systematically studied the spectral and topographical characteristics of muscle contamination in EEG to enhance our understanding of the muscle artifacts. The understanding helped us develop new artifact reduction methods. One of our goals is to follow the effort of Goncharova et al. (2003), and to investigate the characteristics of muscle contaminations under conditions that were not addressed in Goncharova et al. (2003). For example, Goncharova et al. (2003) studied muscle activities with experiments requiring the subjects to intentionally control different parts of their skeletal and facial muscles. In contrast, the muscle activities seen in clinical EEG recordings were primarily due to subjects' unintentional contraction of their muscles. Also, we want to study if, and how, characteristics of muscle contamination change with different EEG recording equipment.

As for muscle artifact reduction methods, human visual rejection of EEG segments with strong muscle artifacts is still one of the most popular methods used, although its insufficiency and infeasibility in many scenarios have been widely documented (Fatourechi et al., 2007). McFarland et al. (1997) proposed using digital filters to automatically identify the EEG segments with strong muscle artifacts for rejection. This approach is only feasible when the EEG signal is redundantly long, and the artifacts happen infrequently. In addition, because muscle artifacts primarily dominate the high frequency range (e.g. the frequency bands of Beta and Gamma), a technique using a low-pass filter was also proposed to remove muscle artifacts. However, it is well known that many important neurological phenomena occur in the high frequency range (Fatourechi et al., 2007). Low-pass filters would remove these neurological phenomena along with the artifacts.

A more promising category of reduction methods is the component-based methods. These methods first decompose a multichannel EEG signal into signal components using a signal decomposition algorithm, such as Blind Source Separation (BSS) (De Clercq et al. 2006), Independent Component Analysis (ICA) (Makeig et al., 1996; Jung et al., 2000; Urrestarazu et al., 2004), or Principle Component Analysis (PCA). After the signal components associated with muscle artifacts, named the *muscle components*, are identified, a muscle-reduced multichannel EEG signal is rebuilt from the remaining non-muscle components. The artifact reduction method proposed in this study belongs to this category of methods.

This method category was probably first introduced by Makeig et al. (1996) to handle generic EEG artifacts, and the Infomax ICA algorithm (Bell and Sejnowski, 1995) was used. De Clercq et al. (2006) proposed a method specially designed to reduce muscle artifacts, called the BSS-CCA method. This method is based upon an assumption that the muscle artifacts are wide-band signals, and thus have smaller autocorrelation. Canonical Correlation Analysis (CCA) was used as the criterion of the BSS signal decomposition algorithm. After the multichannel EEG was decomposed into components ranked by their autocorrelation, a human visual inspection is required to decide the number of the lowest ranked components as the muscle components. However, it is problematic to assume that all muscle artifacts are wide-band signals. Goncharova et al. (2003) demonstrated that at least some categories of muscle artifacts could be narrow-band signals. Moreover, both methods mentioned above require human to identify the muscle components, which hinders their application in high-throughput clinical EEG processing.

Two approaches to evaluate artifact reduction methods exist in the literature. Several studies demonstrated the effectiveness of different artifact reduction methods by subjective visual examination (Jung et al., 2000). In contrast, De Clercq et al. (2006) evaluate their new method using an objective quantitative procedure with the help of realistically simulated EEG data. This paper employs both approaches for method evaluation.

De Clercq et al. (2006) showed that its BSS-CCA method outperformed a component-based method using an ICA algorithm, JADE (Cardoso and Souloumiac, 1993). Our investigation suggested that the failure of that ICA method was primarily because the EEG signals used in De Clercq et al. (2006) were too short for an ICA algorithm to sufficiently decompose them. Their EEG signals have 21 channels, but only have 2500 data points (i.e. 10 s at a sampling rate of 250 Hz). For the relatively small-magnitude muscle activities, this amount of data is insufficient to successfully separate the artifacts from the brain signals. In contrast, when a sufficient amount of EEG data is provided, the success of the ICA methods has been repeatedly shown (Makeig et al., 1996; Jung et al., 2000).

The best method to reduce muscle artifacts in all scenarios may not exist. It will be more informative to clearly specify targeted application scenarios when proposing a new method. The method proposed in this study is designed to efficiently reduce the muscle artifacts in a large amount of multichannel continuous EEG recordings acquired at EEG laboratories worldwide. The EEG signal length, defined as the production of the signal duration and the sampling rate, should be at least ten times the square of the number of channels to ensure sufficient ICA decomposition (Makeig et al., 1996). Also, no EMG channels are required, since different laboratories record the EMG signals at different head locations, using different electrode montages, and with different quality. EEG recordings acquired in many scenarios, including those collected in drug-development clinical trials, meet these criteria.

2. Methods

2.1. Two clinical EEG datasets

EEG datasets collected in two representative clinical trials, CT1 and CT2, are used in this study, and their information is listed in Table 1. Twelve healthy subjects were involved in CT1, while sixteen other healthy subjects were recruited for CT2. In both trials, subjects were instructed to sit in a comfortable chair, relaxing for up to 5 min, and to keep their eyes closed or open during the recording. Forty-eight recordings were collected from each subject under different conditions, such as different visits/periods, different times of the day, etc. Thus, CT1 has 576 5-min recordings, while CT2 has 768 3-min recordings.

The EEG acquisition equipment used in these two trials differs in their amplifier models, electrode placement systems, and system settings. These differences provide us with a chance to study whether equipment has an impact on the characteristics of muscle artifacts. In CT1, the 23 EEG electrodes were attached to subjects' heads one by one. In CT2, Compumedics' *Quik-Cap Electrode Place-*

Table 1
EEG datasets from two representative clinical trials.

Trial name	# Subjects	# Records	# EEG channels	Length (s)	Sampling rate (Hz)	# CO_2 records
CT1	12	576	23	~300	500	0
CT2	16	768	27	~180	512	256

ment System, which is an electrode cap with 27 fixed EEG sensor locations for a subject to wear to locate all electrode positions at the same time. The sampling rate was 500 Hz for CT1 and 512 Hz for CT2. In both trials, neither band-pass filters nor powerline notch filters were used during recording. Also, EMG signals were not collected in either trial. The layouts of the EEG electrodes of both trials follow an extended international 10/20 system of electrode placement (Chatrian et al., 1985).

Goncharova et al. (2003) presented the characteristics of the muscle artifacts under three different EEG electrode reference methodologies, and demonstrated that many artifact characteristics were similar across different references, although some spatial characteristics could be reference-dependent. During recording, CT1 used the linked-ear reference (LER), while CT2 used the unilateral left ear reference (UER) (i.e. all electrodes were referenced to the left eardrop). Our subsequent presentation was primarily based upon the reference of LER due to its popularity in clinical EEG. In addition, recordings using two other references, i.e. UER and common average reference (CAR), were also studied when investigating the spatial characteristics in Section 3.2. Therefore, at the post-processing stage, the recordings of CT1 were re-referenced using UER and CAR, while those of CT2 were re-referenced using LER and CAR to ensure that each recording has three references available for both datasets.

A special design in CT2 is that one third of its 768 EEG recordings were acquired during CO_2 inhalation sessions, in which the subjects closed their eyes, and breathed 5% CO_2 for 3 min when recording EEG. Existing literatures claim that mild and short-period hypercarbia can cause high-frequency EEG activity (Hugelin et al., 1959; Goel et al., 1996; Hemming and Hopkins, 2006), which has been consistently reproduced in our clinical trials. Because the CO_2 inhalation and the muscle artifacts both alter the EEG signals at the high frequency range, the EEG recordings in the CO_2 sessions can be used as an objective probe to examine whether a proposed muscle artifact reduction method can reduce the muscle artifacts, while leaving the CO_2 effect on EEG intact.

2.2. Multichannel EEG decomposition and muscle components

Since the EEG recordings in both datasets were acquired when the subjects were instructed to sit and relax, the muscle activities in the recordings were due to unintentional muscle tensions/activities. It is unclear how the muscle signals produced by unintentional muscle activities are different from those induced by intentionally controlled muscle contractions in Goncharova et al. (2003). At least, the unpredictable nature of the location and strength of the unintentional muscle activities demanded a research approach different from the one adopted by Goncharova et al. (2003).

Our research approach depends on using advanced signal decomposition algorithms to extract the muscle signals from the EEG recordings. Specifically, an N-channel EEG recoding $\mathbf{x}(t)$ is decomposed into N independent signal components using the ICA algorithm of Infomax (Bell and Sejnowski, 1995). Let

$$\mathbf{x}(t) = \mathbf{A}\mathbf{s}(t) + \mathbf{n}(t) = \sum_{i=1}^{N} \mathbf{a}_i s_i(t) + \mathbf{n}(t), \tag{1}$$

where the matrix $\mathbf{A} = [\mathbf{a}_1, \ldots, \mathbf{a}_N]$ and $s(t) = [s_1(t), \ldots, s_N(t)]^T$. That is, $\mathbf{x}(t)$ is decomposed into N independent signal components of $\{\mathbf{a}_i, s_i(t)\}$, $i = 1, \ldots, N$. Each component has two aspects: (1) $s_i(t)$, called the *activation*, represents how the signal component changes in time; (2) $\mathbf{a}_i = [a_1, \ldots, a_N]^T$, called the *spatial vector*, represents how the power of the component distributes across different channels. Signal components that are primarily induced by muscle activities are called the *muscle components*. Therefore, the characteristics of unintentional muscle activities can be studied by investigating these muscle signal components.

After the ICA algorithm was applied to all EEG recordings, for each obtained independent component, the activation signal (i.e. the temporal information), its power spectra (i.e. the spectral information), and its energy distribution across the head (i.e. the spatial information) were plotted out for an EEG expert to examine and decide if the component is a muscle component. For example, under the reference of LER, a total of 3198 signal components were identified as muscle components, among which 1471 were from CT1, and 1727 were from CT2.

2.3. Method to synthesize muscle contaminated EEG data

Because the true muscle-artifact-free EEG signals are unknown in clinical EEG recordings, how well an artifact reduction method can clean up the recordings cannot be objectively and quantitatively evaluated. Using expert-scored muscle artifacts as the ground truth is problematic because they are prohibitively time-consuming to obtain and subject to human biases. A solution is to synthesize realistic muscle-contaminated recordings, $\mathbf{x}_{N\times 1}^{(\lambda,p)}(t)$, from pure EEG signals and muscle activities using Eq. (2):

$$\mathbf{x}_{N\times 1}^{(\lambda,p)}(t) = \mathbf{b}_{N\times 1}(t) + \lambda \begin{bmatrix} \beta_1^{(p)} & & \\ & \ddots & \\ & & \beta_N^{(p)} \end{bmatrix} \mathbf{m}_{N\times 1}(t) \tag{2}$$

where N is the number of channels; $\mathbf{b}_{N\times 1}(t)$ denotes the pure muscle-free N-channel EEG signals; $\mathbf{m}_{N\times 1}(t)$ denotes N muscle signals randomly selected from a pool of representative muscle signals, such that the power of each muscle signal in $\mathbf{m}_{N\times 1}(t)$ is scaled to be equal to that of the EEG signal at channel Pz in $\mathbf{b}_{N\times 1}(t)$ (Channel Pz is selected because it is less subject to ocular and muscle artifacts.); $\beta_i^{(p)} \in \{0, 1\}, i = 1, \ldots, N$, are independent Bernoulli random variables with a parameter $p \in [0, 1]$, and a bigger p leads to more muscle-contaminated channels in $\mathbf{x}_{N\times 1}^{(\lambda,p)}(t)$; and $\lambda \in [0, 1]$ is a factor to control the relative strength of the muscle contamination. The bigger λ is, the stronger the muscle contamination is.

To prepare $\mathbf{b}_{N\times 1}(t)$, the EEG recordings in both CT1 and CT2 were visually examined. Seven recordings without visible muscle artifacts and with minimal other artifacts are selected. Three of these seven recordings were from three different subjects in CT1, while the remaining four recordings were from three different subjects in CT2. The selected recordings were further processed to remove signal baseline drafts. The cleaned recordings are used as $\mathbf{b}_{N\times 1}(t)$ in (2).

Both Goncharova et al. (2003) and our extensive observation suggested that the muscle signals induced by unintentional muscle activities were heterogeneous. However, the exact number of the major categories of muscle signals is challenging to know because the muscle signals are frequently induced by the joint muscle activities from several muscle sources, and thus their difference

is not clear-cut. Ideally, the pool of candidate muscle signals to form $\mathbf{m}_{N\times1}(t)$ in (2) should represent different major categories of the muscle components. A clustering procedure was used to achieve this goal. More specifically, those 3198 muscle components extracted in Section 2.2 were clustered into 10 clusters based on their Power Spectral Density (PSD) profiles using the *k*-means clustering method (Seber, 1984). The choice of 10 clusters is partially due to practical considerations such as computation, human review efforts, etc. It is subsequently justified as a sensible choice for our purpose in Section 3.1. The muscle component that is closest to the centroid of each cluster is selected as the representative muscle component of that cluster. The activations of the selected representative muscle components were then filtered by a high-pass filter with a transition band from 5 to 8 Hz. The pool of 10 representative muscle signals was formed from these processed activations to be used as the candidate muscle signals to form $\mathbf{m}_{N\times1}(t)$ in (2).

For each of the seven prepared $\mathbf{b}_{N\times1}(t)$'s, Eq. (2) was applied four times to generate four different simulated EEG recording, $\mathbf{x}_{N\times1}^{(\lambda,p)}(t)$, because the $\mathbf{m}_{N\times1}(t)$ and $\beta_i^{(p)}$ are different each time. Given a pair of parameters λ and p, 28 simulated recordings were thus synthesized, among which 12 were based on recordings from CT1, while 16 were based on recordings from CT2. Four pairs of parameters λ and p are used in this study: ($\lambda = 0.5$, $p = 0.08$), ($\lambda = 0.5$, $p = 0.5$), ($\lambda = 0.9$, $p = 0.08$), and ($\lambda = 0.9$, $p = 0.5$). These four pairs represent four different scenarios. For example, the pair of ($\lambda = 0.5$, $p = 0.08$) generate recordings that have on average 8% channels contaminated with relatively weak (i.e. half EEG signal magnitude) muscle artifacts. Finally, 48 simulated recordings that are based on the pure EEG signals $\mathbf{b}_{N\times1}(t)$ from CT1 formed the simulated dataset of CT1-Sim, while the CT2-Sim dataset has 64 simulated recordings.

2.4. An efficient muscle artifact reduction method

A muscle-reduced EEG recording can be constructed using Eq. (1), if we set the activations $s_i(t)$ of the muscle components to zero. The remaining issue is how to decide which signal components are the muscle components. Visually reviewing each signal component can be time-consuming when handling the clinical EEG recordings. For example, we need to review 33,984 signal components (see Table 1 as $23 \times 576 + 27 \times 768 = 33{,}984$) to process the recordings in CT1 and CT2. Therefore, this study proposes a method to automatically and effectively identify muscle components.

After studying tens of thousands of signal components obtained from thousands of EEG recordings acquired under different scenarios, a distinguishing characteristic of the muscle components that we observed is that some high-frequency segments of their PSD profiles maintain flatness, or even increase, while the PSDs of other EEG signal components almost always decrease at the frequency range above 40 Hz. A simple biophysical explanation to this observation is that, before being captured by EEG sensors on scalps, brain signals generated in the cortex pass several layers of brain anatomical structures, which jointly act as a wide-transition-band low-pass filter to attenuate signal power proportionally to the frequency. In contrast, the muscle activities occur at the surface of the head, and thus can retain fairly strong signal power in the high-frequency range. This observation aligns with the results in Goncharova et al. (2003).

Based on this observation, an effective and robust feature to automatically differentiate muscle components from other signal components is proposed after further considering different categories of muscle signals. The muscle feature, which is called the *Spectral Ratio* (SR) feature, is formulated in Eq. (3). Let

$$\log\{H(S_i(f))/L(S_i(f))\}\begin{cases}\leqslant\Delta & \rightarrow \text{non-muscle}\\ >\Delta & \rightarrow \text{muscle}\end{cases} \tag{3}$$

where $S_i(f)$ is the power spectra of $s_i(t)$; $H(S_i(f)) = \frac{1}{|f\in[40,60]|}\sum_{f\in[40,60]}S_i(f)$ denotes the mean of the power spectra $S_i(f)$ over a high-frequency range between 40 and 60 Hz; $L(S_i(f)) = \min_{f\in[4,30]}(\mathbf{F}_{\text{smooth}}\otimes S_i(f))$ denotes the smallest value over a low-frequency range between 4 and 30 Hz of a smoothed version of the power spectra Si(f), where $\mathbf{F}_{\text{smooth}}$ is a moving average smooth filter, and $\otimes$ is the convolution operator.

Since the proposed method uses ICA to decompose the EEG signals, and uses the SR feature in (3) to automatically identify muscle components, it is referred to as the ICA-SR method subsequently.

The threshold Δ in (3) is a pre-specified, non-negative algorithmic parameter, whose non-negativity implies that $H(S_i(f)) \geq L(S_i(f))$. The simulated datasets generated in Section 2.3 are used to investigate the impact of this parameter. The muscle-free EEG signal $\mathbf{b}(t)$ is known for the simulated EEG recordings, and the criterion of minimizing Mean Squared Error (*MSE*), defined in Eq. (4), is used to help us search for an optimal default value of Δ, and the results are illustrated in Fig. 1. Let

$$MSE(\Delta) = MSE_m(\Delta) + MSE_c(\Delta) \tag{4}$$

where $MSE_m(\Delta) = \frac{1}{n|T|}|\mathbf{M}\sum_{t\in T}(\mathbf{b}(t) - \hat{\mathbf{b}}(t|\Delta))^2$ is the *MSE* between the muscle-free EEG signal $\mathbf{b}(t)$ and the muscle-reduced signal $\hat{\mathbf{b}}(t|\Delta)$ for the muscle-contaminated channels, $MSE_c(\Delta) = \frac{1}{(N-n)|T|}(1-\mathbf{M})\sum_{t\in T}(\mathbf{b}(t) - \hat{\mathbf{b}}(t\mid\Delta))^2$ is the *MSE* for the channels that were not contaminated by muscle artifacts when synthesizing the simulated recording, where T is the time duration of the recording, $|T|$ is the number of time points in T, $\mathbf{M} = [m_1,\ldots,m_N]$, where $m_i = 1$ when the ith channel is muscle contaminated, otherwise $m_i = 0$; and $n = \sum_{i=1}^{N} m_i$ is the number of channels that are muscle contaminated.

The four curves in Fig. 1 illustrate the results of four sets of simulated muscle-contaminated recordings respectively. The proposed ICA-SR method is applied to the four sets of recordings when the threshold Δ is set from 0 to 0.6. MSE_m (Δ), MSE_c (Δ), and their combination, i.e. $MSE(\Delta)$, are averaged within each set of recordings, and then plotted over the threshold in the left, middle, and right panels, respectively. The combined *MSE* is used to identify the optimal default threshold, which is indicated using a vertical dotted line in the right panel. Minimal $MSE(\Delta)$ is achieved at the default value.

Fig. 1 illustrates that Δ balances between MSE_m (Δ) and MSE_c (Δ). The smaller Δ is, the more signal components are identified as muscle components for removal, and the cleaner the muscle-contaminated channels are (i.e. the smaller MSE_m (Δ) is). In contrast, the bigger Δ is, the fewer signal components are identified as muscle components, and the less distortion is introduced to the muscle-free channels (i.e. the smaller MSE_c (Δ) is). MSE_m (Δ) is generally much larger than MSE_c (Δ) in values. Also, the *MSEs* are more sensitive to the choice of Δ when many channels have weak muscle contaminations, e.g. the scenario of ($\lambda = 0.5$, $p = 0.5$). Fig. 1 suggests that the default value of Δ should be 0.08.

After the muscle components are identified using Eq. (3), it is more beneficial to partially remove the activation $s_i(t)$ of a muscle component, instead of setting the whole activation $s_i(t)$ to zero, because the muscle signals primarily alter the signal at the high frequency range (Goncharova et al., 2003). This partial removal is implemented by applying a Finite Impulse Response (FIR) low-pass filter with a cutoff frequency of 16 Hz, which removes the high frequency part of the muscle signals, but leaves their low frequency part intact. After that, both the partially cleaned muscle components and the other signal components are input into Eq. (1) to reconstruct a muscle-reduced EEG recording.

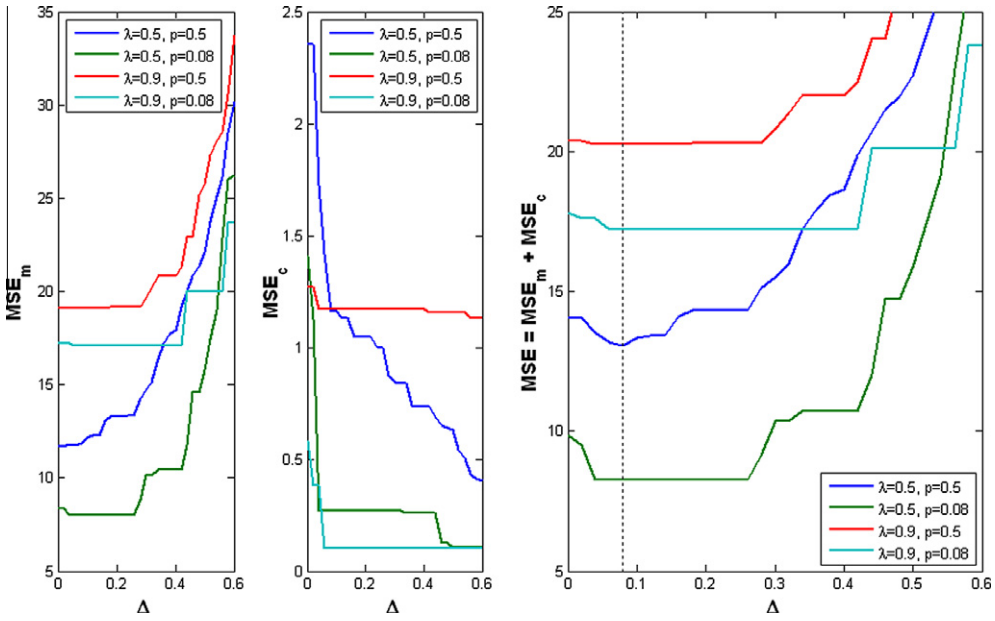

Fig. 1. Finding the optimal default value of the threshold Δ.

3. Results

3.1. Spectral and temporal characteristics of unintentional muscle activities

In Section 2.3, the 3198 muscle components extracted from datasets CT1 and CT2 were clustered to identify 10 representative muscle signals. This procedure heuristically ensures that these representative muscle signals are both different from each other, and meanwhile cover a range of major diversity of the muscle components. Therefore, these representative muscle signals provide an overview of the heterogeneous characteristics of the muscle components in both the time and frequency domains.

The frequency-domain power spectra of these muscle signals are shown in Fig. 2(a), while their 5-s snapshots in the time domain are shown in Fig. 2(b). Only the power spectra above 8 Hz were plotted in Fig. 2(a), since the muscle artifacts primarily alter the power spectra at the high frequency range. The dashed lines in Fig. 2(a) illustrate the means of each power spectra.

Some representative muscle signals are visually more distinct than the others. It is interesting to observe that, out of these 10 muscle signals, three signals have relatively more distinct spectral or temporal characteristics, and they happen to match the three muscle patterns presented in Goncharova et al. (2003). Specifically, the representative muscle signals 2, 9, and 10 are fairly close to the "Railroad cross-tie" pattern, the "noise-like" pattern, and the "Beta rhythm-like" pattern in Goncharova et al. (2003), respectively.

The representative muscle signals 5 and 6 are similar to each other at both the frequency and the time domains. They are likely from the subcategories of one major category of muscle signals. This implies that the number of major muscle categories could be smaller than 10. Therefore, when we set the number of clusters as 10 in Section 2.3, some major categories ended up being split into their subcategories. This suggests that our choice of 10 clusters is sufficient to avoid folding several major categories into one cluster.

3.2. Spatial characteristics of unintentional muscle activities

Each independent muscle component, i.e. {**a**, $s(t)$}, is composed of a muscle activation signal $s(t)$, and a muscle spatial vector **a**. The activation signal $s(t)$ has been studied in Section 3.1 when investigating the spectral and temporal characteristics of the muscle artifacts. This subsection focus on the muscle spatial vector a, which indicates how the power of the component distributes across electrodes at different scalp locations, i.e. the spatial characteristics of the muscle artifacts.

An EEG recording's reference methodology affects the relative signal strength at different channels (i.e. electrodes). A natural question is whether the spatial characteristics of the muscle artifacts are also reference-dependent. To address this question, recordings under three references, i.e. UER, LER, and CAR, are decomposed using the ICA algorithm, and the muscle components are selected. As for dataset CT1, 1648, 1471, and, 1953 muscle components were identified for references of UER, LER, and CAR, respectively. As for dataset CT2, 1829, 1727, and 1703 components were identified for the three references, respectively. After the spatial vector of each component was normalized, the spatial vectors from each dataset were averaged to obtain the group-level spatial vector of those unintentional muscle activities for each dataset and under each reference methodology. The averaged spatial vector in CT1 is shown in the first row in Fig. 3 (i.e. (a), (b), and (c)), while that in CT2 is shown in the second row (i.e. (d), (e), and (f)). The three columns in Fig. 3 are corresponding to the three reference methodologies: UER (i.e. (a) and (d)), LER (i.e. (b) and (e)), and CAR (i.e. (c) and (f)). The form of visualization in Fig. 3 is called the *muscle activity topography*.

Results of both datasets demonstrated that the spatial characteristics of the three references are fairly similar to each other, which suggests that our approach captured the spatial characteristics that are insensitive to the three references used. The details of the EEG signals were studied, which revealed that, although these reference methodologies changed the relative magnitudes of the EEG signals, they did not significantly alter the proportion of muscle artifacts at different channels. More and stronger muscle artifacts more likely occur in the EEG channels where more head muscles exist.

Results from both datasets and three references suggested that the strongest muscle activities happened around the temporal areas, and some muscle activities also happened at the frontal areas. This makes senses because the head muscles exist in these areas.

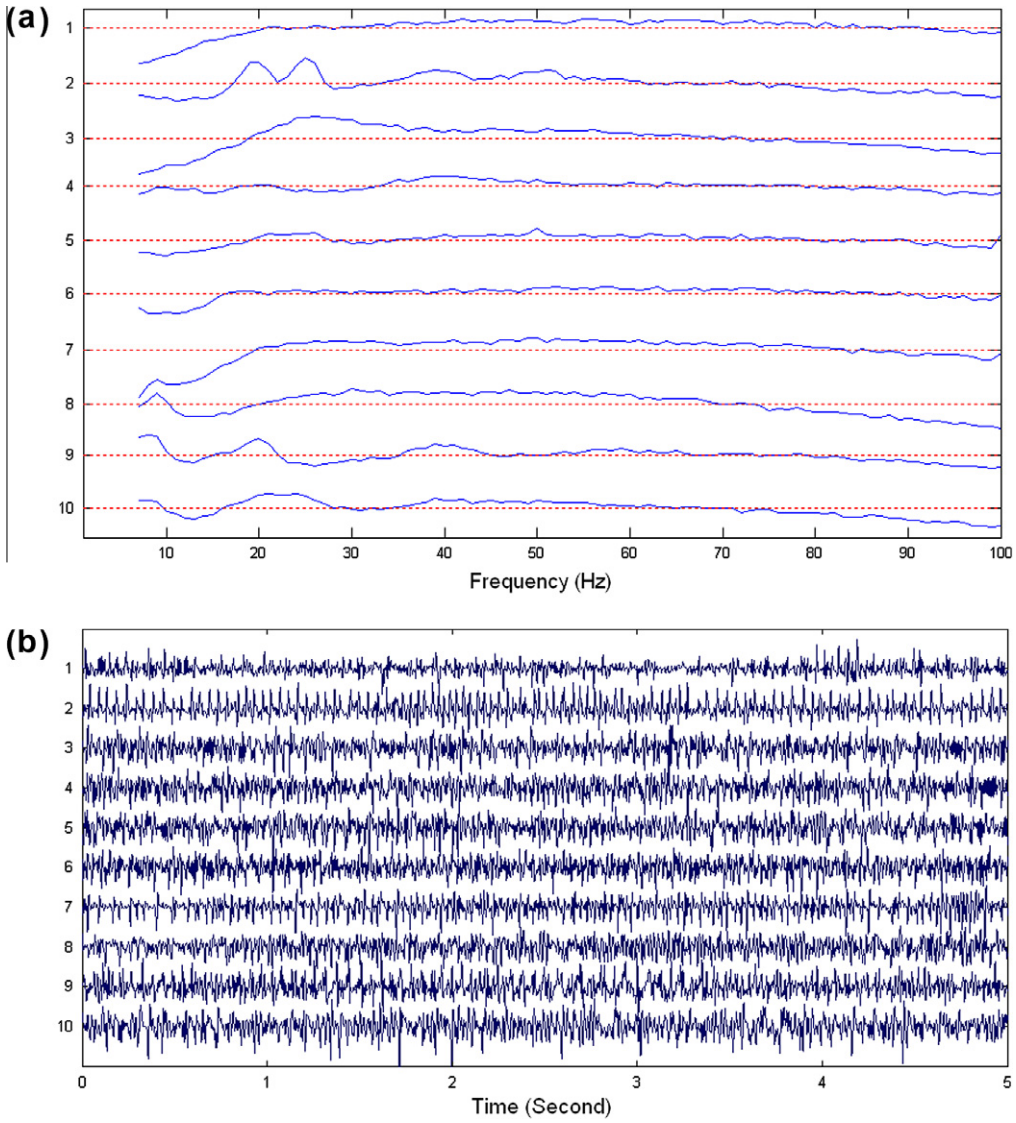

Fig. 2. The spectral and temporal plots of the 10 representative muscle signals.

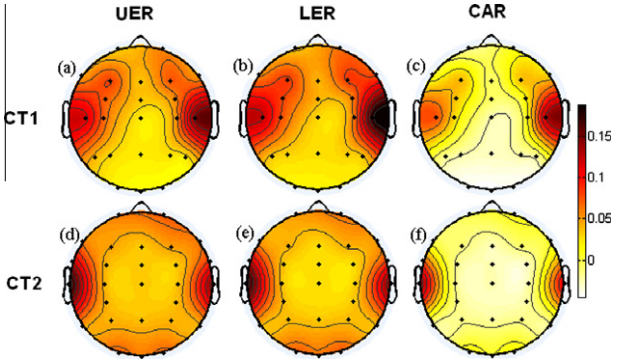

Fig. 3. The topographies to illustrate the averaged spatial distribution of the muscle activities. UER is the short for "unilateral left ear reference", LER is for "linked-ear reference", and CAR is for "common average reference".

A major difference between CT1 and CT2 is that CT2 has much stronger muscle activities in the occipital area. Using a two-sample *t*-test, the null hypothesis that the occipital areas of two datasets are the same was rejected with a *p*-value nearly zero for all three references. Detailed statistical analysis results are presented in Table 2.

The reason for this very significant difference at the occipital area was due to the different electrode placement systems used in these datasets. In CT1, the EEG electrodes were attached to subjects' heads one by one, while an electrode cap was used for electrode placement in CT2. The electrode cap is likely to cause muscle tension at the occipital area if the shape of the cap and that of the subject's head do not comfortably match.

For brevity, only the data under the reference of LER were presented subsequently.

The spatial characteristics shown in Fig. 3 are the group-level properties obtained by averaging over all subjects' muscle components. In fact, each subject can have his/her spatial characteristics that are distinguishing from the group spatial characteristics. In CT1, each of the 12 subjects can generate 1104 independent signal components (i.e. 48 recordings/subject $\times$ 23 components/recording = 1104), while in CT2, each of the 16 subjects can generate 1296 independent components (i.e. 48 recordings/subject $\times$ 27 components/recording = 1296). The muscle components of a subject can be averaged and visualized as this subject's muscle activity topography. The muscle activity topographies at the subject-level

Table 2
Occipital area comparison between CT1 and CT2. UER is the short for "unilateral left ear reference", LER is for "linked-ear reference", and CAR is for "common average reference". SE is the short for "standard error of the mean".

Reference method	Data set	Mean (SE)	CT2 vs. CT1				
			t-Stat	d.f.	*p* value	Mean diff.	95% Conf. int.
UER	CT1	0.017(0.002)	11.49	3475	0.000	0.053	(0.044, 0.063)
	CT2	0.071(0.004)					
LER	CT1	0.020(0.002)	10.94	3196	0.000	0.053	(0.043, 0.062)
	CT2	0.073(0.004)					
CAR	CT1	−0.042(0.002)	12.11	3279	0.000	0.060	(0.050, 0.069)
	CT2	0.018(0.004)					

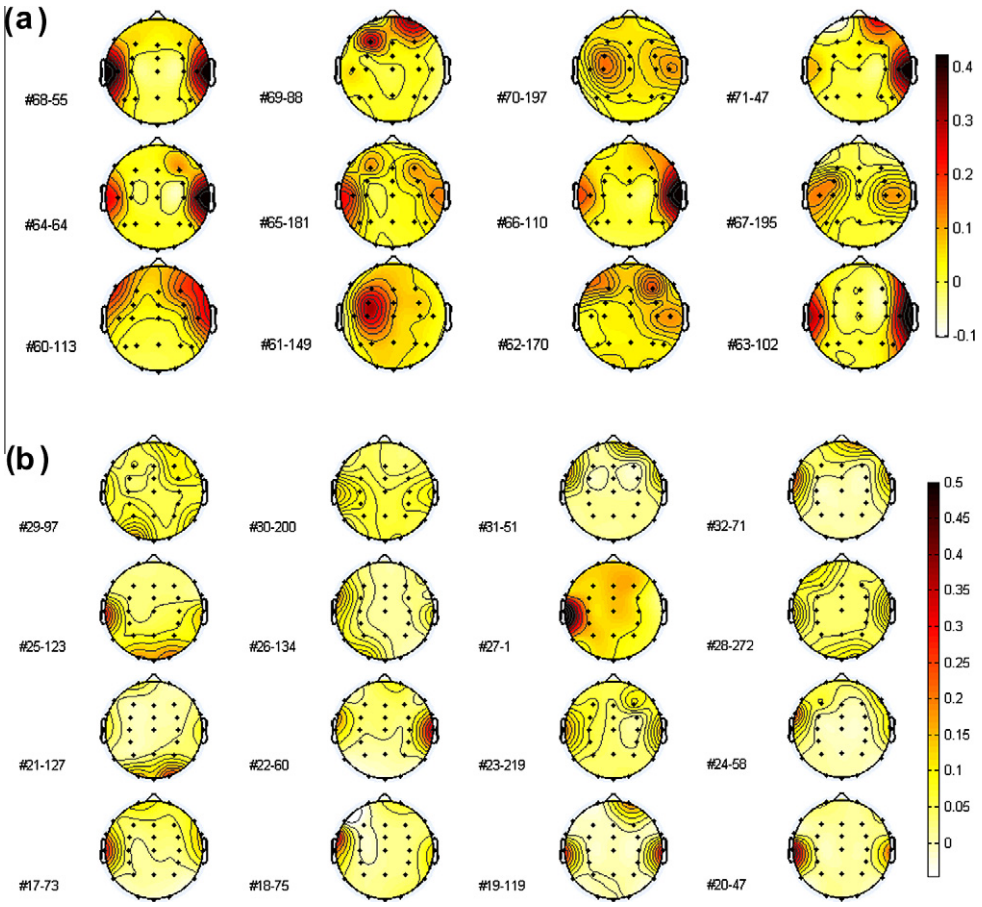

Fig. 4. The subject-level topographies to illustrate the spatial distribution of muscle activities for each subject.

for CT1 are shown in Fig. 4(a), and those for CT2 are shown in Fig. 4(b). Each subject's muscle activity topography was labeled with that subject's ID, along with the number of identified muscle components from this subject. For example, the label of the first muscle activity topography is "#68-56", which means that 56 components out of the 1104 independent components from subject #68 in CT1 were identified as muscle components, and this subject's spatial vector is obtained by averaging over the 56 muscle components.

Fig. 4 shows that the muscle spatial characteristic at the subject-level can be very different from that at the group-level. Also, some subjects had very strong and complex muscle activities, and generated many muscle components. For example, subject # 28 in CT2 had 272 muscle components, which accounts for 21% of his/her signal components. In contrast, some subjects have very few and simple muscle activities. For example, subject #27 in CT2 only has 1 muscle component out of his/her 1296 signal components. Another observation is that the strongest muscle activities in CT2 always happened at the edge of the head. This is however not the case in CT1. Again, this difference can also be because the edge of the electrode placement cap used in CT2 can irritate the subjects' heads to cause certain unintentional muscle tension.

Fig. 4(b) shows that, different from the group-level results in Fig. 4(b), some subjects in CT2, such as subjects #17, #20, #22, #24, #31, and #32, have very little muscle activities in the occipital areas. Meanwhile, some subjects had very strong occipital muscle activities, such as subject #21, #25, and #28. One explanation is that some subjects' caps fit their head better than the others'. Similarly, Fig. 4(a) shows that, as opposed to the group-level results in Fig. 4(a), some light occipital muscle activities indeed occurred in a few subjects in CT1, such as subjects #61, and #62.

No occipital muscle activities were reported in Goncharova et al. (2003) because no experiment was designed to control occipital muscles in that study. However, our results suggested that

occipital muscle activities can unintentionally happen during EEG recording for some subjects.

3.3. Objectively evaluating the ICA-SR method using simulated EEG recordings

Although the muscle artifact reduction method of BSS-CCA (De Clercq et al. (2006)) requires humans to decide the number of muscle components, it is one of the few promising methods available in the literature that has a potential application in high-throughput EEG data processing. An objective comparison between ICA-SR and BSS-CCA was conducted using the simulated datasets in Section 2.3.

The criteria of MSE_m and MSE_c defined in Eq. (4) are used to objectively and quantitatively compare both methods. The pure EEG signal $\mathbf{b}(t)$ and the contaminated channels $\mathbf{M}$ are known when the recording is synthesized, while the muscle-reduced EEG signal $\hat{\mathbf{b}}(t)$ can be obtained by inputting the simulated recording into both methods. The smaller the value, the better the method is. The results are listed in Table 3. In each comparison, the favorable result is bolded. Table 3 shows that, except for one scenario, the ICA-SR method clearly outperformed the BSS-CCA method under both criteria. That is, ICA-SR restored the true EEG signals better in the muscle-contaminated channels, while introducing less distortion in the non-contaminated channels.

3.4. Evaluating the ICA-SR method's ability to process clinical EEG recordings in a high-throughput fashion

One of our goals is to develop a muscle-reduction method that requires minimal human intervention when processing large clinical EEG datasets in a high-throughput fashion. In order to evaluate the proposed ICA-SR method, we set the only algorithmic parameter Δ in (3) to 0.08, as suggested by Fig. 1. The 1344 EEG recordings from both datasets CT1 and CT2 were fed into the ICA-SR method in a batch mode without any human intervention. It took a workstation (dual Intel-quad-core Xeon 2.27 GHz CPUs, 6 GB RAM, and the 64-bit Windows 7 Professional operation system) about 22.5 h to finish this task.

Since the true EEG signal is unknown in this context, a sensible approach is to visually compare the outputted muscle-reduced EEG recordings with the corresponding original recordings to check whether the method sufficiently reduces the muscle artifacts, and meanwhile leaves the non-contaminated EEG channels intact. We visually reviewed the recordings one by one, and confirmed that the ICA-SR method successfully reduced the muscle artifacts in most of the recordings. Two samples are illustrated in Fig. 5.

Two 3-s snapshots of two CT2 recordings from subject #30 at period 1, time 1, and eye-closed condition (both before and after applying the ICA-SR method) are shown in Fig. 5(a) and (b), respectively. The difference between these two recordings is that the recording in Fig. 5(b) was acquired during the 5% CO_2 inhalation session. Fig. 5(a) shows that channels Oz and O1 were contaminated by muscle artifacts in the original signals, while almost no muscle artifacts could be observed after applying the ICA-SR method. Fig. 5(b) shows that many channels (e.g. T7, T8, P7, P8, and C3) were contaminated by strong muscle artifacts in the original signals, while the strong muscle artifacts disappeared after applying the ICA-SR method. Fig. 5(b) also shows that some channels (e.g. CP4) were mildly and sparsely contaminated, in which case the artifacts could still be somewhat seen after applying the ICA-SR method. This suggests that the ICA-SR method can sometimes miss some mild muscle artifacts. Unfortunately, this issue also happens to other component-based methods, e.g. the BSSS-CCA method. Therefore, it is more appropriate to call these methods artifact-reduction, instead of artifact-removal, methods.

Fig. 5(c) illustrates the impact of the ICA-SR method on three representative channels at the frequency domain by comparing their PSDs before and after applying the ICA-SR method, along with the conditions of No-CO_2 and CO_2. The upper panel of Fig. 5(c) compares the PSDs of channel O1, a channel with strong muscle-contamination. The PSDs before applying the ICA-SR method have no difference between the conditions of CO_2 and No-CO_2 because the muscle artifacts dominate the effect of CO_2 inhalation. The CO_2 effect is revealed after the muscle artifacts are reduced by the ICA-SR method. The middle panel of Fig. 5(c) compares the PSDs for channel Pz, a channel with mild muscle contamination. The lower panel compares the PSDs for channel Cz, a channel almost without muscle contamination. Overall, Fig. 5(c) demonstrates that the CO_2 effect becomes more consistent after the muscle artifacts are reduced using the ICA-SR method.

As shown in Fig. 5(c), muscle artifacts primarily alter the EEG signals at the high frequency range, while the effect of CO_2 inhalation on EEG signals affects the EEG signals almost at the same high frequency range. An ideal reduction method should maintain the CO_2 effect while reducing the muscle artifacts. Comparing the estimated CO_2 effects before and after applying the ICA-SR method allows us to objectively evaluate the proposed method from a different perspective.

The CO_2 effect at the Gamma band (i.e. 24–60 Hz) is investigated because it is the frequency band that was strongly influenced by both muscle artifacts and the CO_2 inhalation. Since each subject has multiple repeated EEG recordings, a linear mixed-effects statistical model (Pinheiro and Bates, 2000) with the subjects as the random effect was used to estimate the CO_2 effect of that channel. The results are shown in Fig. 6. The markers indicate the estimated CO_2 effects, while the vertical bars around the markers indicate the 95% Confidence Intervals (CIs) of the estimated effects. The estimated CO_2 effects before and after applying the ICA-SR method are compared side-by-side for each channel. The horizontal line at 0.0 indicates the scenario when no CO_2 effect exists. Since the CIs of all channels are above the horizontal line, Fig. 6 demonstrates that the CO_2 effect, which increases the EEG power spectra at the Gamma band, is maintained before and after applying the ICA-SR method. The magnitude of the estimated effects are similar across all channels except for the three channels of T7, T8, and P7, whose

Table 3
An objective comparison of ICA-SR and BSS-CCA base on the Mean Squared Error (*MSE*) between the original EEG and the muscle-reduced EEG.

			$\lambda = 0.5$, $p = 0.5$	$\lambda = 0.5$, $p = 0.08$	$\lambda = 0.9$, $p = 0.5$	$\lambda = 0.9$, $p = 0.08$
MSE_m	CT1-sim	ICA-SR	**5.7601**	**3.8443**	**7.9647**	**7.7311**
		BSS-CCA	16.0943	15.2123	16.9280	17.0271
	CT2-sim	ICA-SR	**6.1263**	**4.1448**	**11.1421**	**9.3804**
		BSS-CCA	15.4282	14.0622	14.4741	13.8456
MSE_c	CT1-sim	ICA-SR	1.7737	**0.3352**	**0.4990**	**0.0996**
		BSS-CCA	**0.7502**	0.4178	0.8559	0.6285
	CT2-sim	ICA-SR	**1.4890**	**0.5470**	**1.3380**	**0.4821**
		BSS-CCA	5.1034	2.2785	2.5203	1.8833

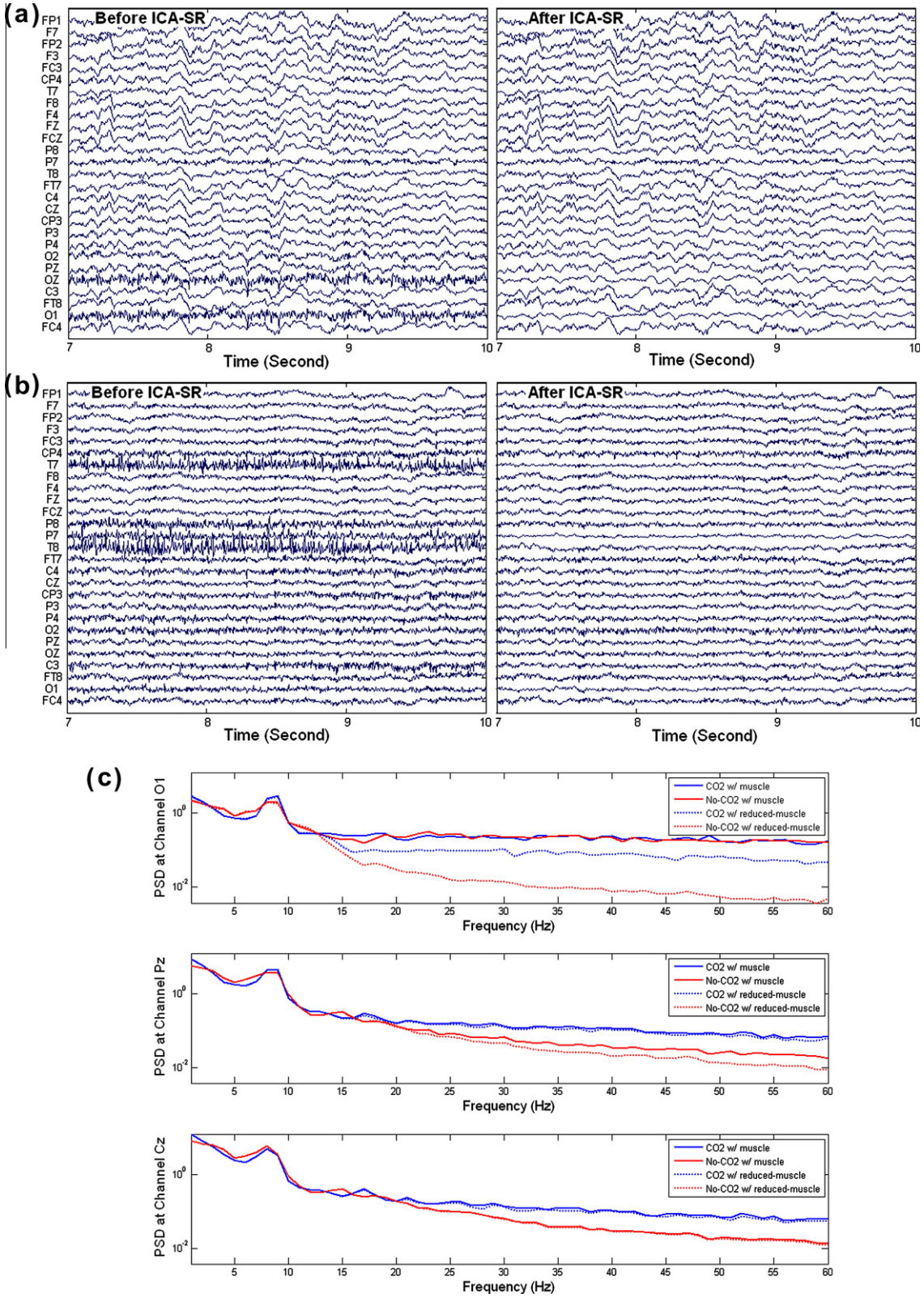

Fig. 5. Comparison of real EEG recordings before and after applying the ICA-SR method in the time and the frequency domains.

estimated effects are statistically significant different before and after applying the ICA-SR methods. These channels happen to be those most vulnerable to muscle artifacts, as shown in Fig. 3(e). Before applying the ICA-SR method, the estimated CO_2 effects of these channels are much larger than those of the other channels. This is suspicious because the CO_2 inhalation incurs a global effect across the whole head, and no biological reasons support that its effects at the temporal area should be especially stronger than at other head areas. After applying the proposed method, the CO_2 effects of these channels become more consistent with those of

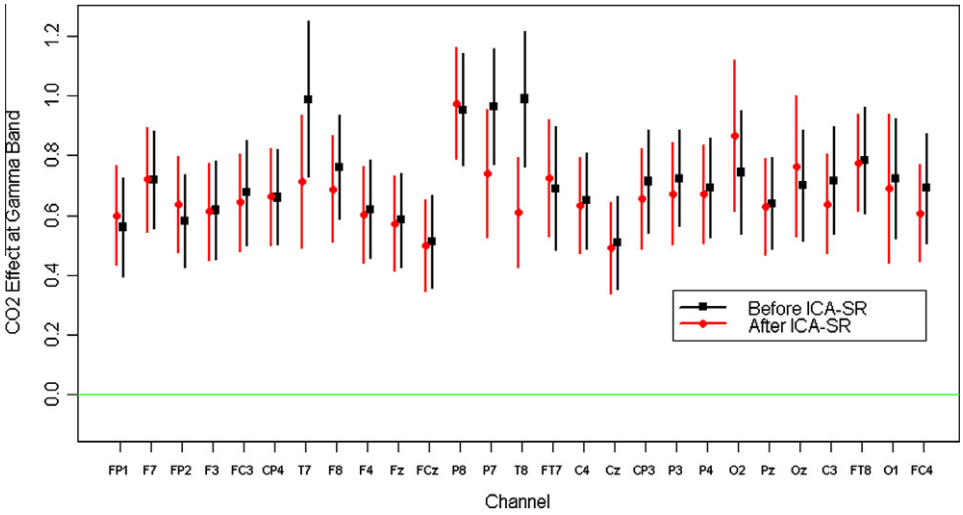

Fig. 6. The estimated CO_2 effects at the Gamma Band (24–60 Hz) before and after applying the ICA-SR method.

the other channels. This observation suggests that the ICA-SR method leads to more sensible estimates of the CO_2 effects at the most muscle-contaminated channels, and meanwhile it generally maintains the estimates of the CO_2 effects in the other channels.

4. Discussion and conclusion

This study focused on the unintentional muscle artifacts occurring in general clinical EEG recordings. The reported spectral, temporal, and spatial characteristics of the muscle activities confirmed, and meanwhile expanded, our knowledge of muscle contaminations in EEG. In addition, a muscle-reduction method, i.e. the ICA-SR method, was proposed and evaluated. This method provides us with an urgently needed tool for processing continuous multichannel clinical EEG recordings in a high-throughput fashion with validated performance. One of the future efforts is to evaluate the efficacy of the proposed method in different specific therapeutic areas. For example, it is recommended to evaluate whether the method can preserve the EEG morphology of electrographic seizure activity, since the muscle artifacts frequently make interpretation difficult in this scenario.

4.1. Pre-processing of the EEG data is critical for component-based methods

The success of any component-based artifact reduction methods depends on how well the artifacts are decomposed as isolated signal components. If the decomposition algorithm produce signal components that have both artifacts and true EEG signals, removing these mixture components will lead to a loss of EEG signal, while keeping these components will retain the artifacts. Usually, if the EEG recordings have *N* channels, the ICA algorithm can at most decompose EEG into *N* independent signal components. If more than *N* independent signal sources are embedded in EEG, the ICA algorithm first outputs signal components with strong independent sources, then it has to pack several weaker independent sources into one signal component.

Many ICA algorithms, including the Infomax ICA implemented in the EEGLab toolbox (Delorme and Makeig, 2004), are sensitive to large peak artifacts, and strong power-line frequency interference, and used many signal components to describe these strong but simple-to-remove artifacts. Therefore, before applying any component-based artifact reduction methods, a simple automatic pre-processing procedure should always be applied to first remove those large peak artifacts and the strong power-line frequency interference in the EEG recordings (Anderer et al., 1999). This pre-processing gives the subsequent decomposition algorithm a better chance to produce signal component with either purer artifacts or purer true EEG.

4.2. The muscle activity topography generated by the ICA-SR method can help to detect the stressful spots on a person's head

The ICA-SR method can automatically process a person's EEG recordings and generate his/her muscle activity topography like those in Fig. 4 within 1 min. The muscle activity topography directly visualizes the spots on a person's head where his/her muscles unintentionally contract. This capability potentially creates extra usages of the ICA-SR method. For example, the results from CT2 suggest that the uncomfortable mismatch between the electrode placement cap and a person's head can lead to excessive muscle artifacts around the mismatched spots. Therefore, the muscle activity topography generated by the ICA-SR method can be used to identify those mismatches.

Another application of the ICA-SR method is to help a person better relax. EEG recordings in CT1 and CT2 were acquired when the subjects were instructed to sit and relax. However, the EEG recordings still showed that some subjects had constant and fairly strong muscle activities at some spots of the head. We noticed that, in some instances, these unintentional muscle activities disappeared when the subjects fully relaxed to the extent of falling asleep. The unintentional chronic muscle stresses can have a negative impact on a person's health. The muscle activity topography might be used as a biofeedback tool. It will be easier for the subject to intentionally relax those stressful spots, if the stressful spots are visualized to him/her.

4.3. Conclusions are drawn under certain conditions

Fig. 3 shows that, compared with CT1, the electrode placement caps used in CT2 introduced a considerably larger amount of muscle artifacts at the occipital area. That is, the characteristics of the muscle activities can be equipment-related. If our study had only used one EEG dataset, or datasets acquired using the same EEG equipment, we might make general statements regarding the spatial characteristics of the muscle activities, which are actually equipment-specific. Unfortunately, this is a fairly common pitfall in the literatures in this research community.

This reminds us that, when reporting a study, researchers should always present the detailed technical conditions of the study, e.g. EEG acquisition equipment, EEG reference methodology, operation procedure, subject cohort selection, data analysis procedure, etc. Meanwhile, when the conclusions from the literatures are cited, the conditions, under which the conclusions are drawn, should always be considered.

4.4. Human review is indispensable when processing clinical EEG data

The proposed method was designed as a high-throughput method to minimize human involvement in EEG signal processing. However, because many unexpected scenarios can happen in real-world clinical settings, it is very challenging to prepare an automatic program that can handle all unusual cases properly. Therefore, a human review of the processed results is always strongly recommended. Fortunately, this down-stream human review is much easier than the up-stream human artifact detection done at the raw signal level.

Besides muscle artifacts, several other major artifacts exist in clinical EEG datasets. Thus, clinical EEG processing usually requires a comprehensive system to handle all major artifacts. In addition to the proposed method to efficiently reduce muscle artifacts, high-throughput methods designed to handle other major artifacts should also be incorporated in the system (Ma et al. 2011). In this scenario, instead of reviewing the results after each automatic method, one final human review at the end of the whole system is generally sufficient. Therefore, the demand for human review is normally an attainable requirement.

Financial interests

This study was done by Merck employees, and by researchers funded by Merck & Co. Inc.

Acknowledgements

The authors would like to thank Dr. Christopher Tong for helpful discussions about the manuscript. Also, the authors want to thank the clinical team for generating the two clinical EEG datasets. In addition, the authors would like to thank the reviewers and the editor, whose inputs significantly improved this manuscript.

References

Anderer P, Roberts S, Schlögl A, Gruber G, Klösch G, Herrmann W, et al. Artifact processing in computerized analysis of sleep EEG – a review. Neuropsychobiology 1999;40:150–7.

Barlow JS. Artifact processing (rejection and minimization) in EEG data processing. In: Lopes da Silva FH, Storm van Leeuwan W, Remond A, editors. Handbook of electroencephalography and clinical neurophysiology. Revised series 1986;vol. 2. Amsterdam: Elsevier; 1986. p. 15–62.

Bell AJ, Sejnowski TJ. An information-maximization approach to blind separation and blind deconvolution. Neural Computation 1995;7:1129–59.

Cardoso JF, Souloumiac A. Blind beamforming for non Gaussian signals. IEE Proc – F Radar Signal Processing 1993;140:362–70.

Chatrian GE, Lettich E, Nelson PL. Ten percent electrode system for topographic studies of spontaneous and evoked EEG activity. Am J EEG Technol 1985;25:83–92.

De Clercq W, Vergult A, Vanrumste B, Van Paesschen W, Van Huffel S. Canonical correlation analysis applied to remove muscle artifacts from the electroencephalogram. IEEE Trans Biomed Eng 2006;53:2583–7.

Delorme A, Makeig S. EEGLAB: an open source toolbox for analysis of single-trial EEG dynamics. J Neurosci Methods 2004;134:9–21.

Fatourechi M, Bashashati A, Ward RK, Birch GE. EMG and EOG artifacts in brain computer interface systems: a survey. Clin Neurophysiol 2007;118:480–94.

Goel V, Brambrink AM, Baykal A, Koehler RC, Hanley DF, Thakor NV. Dominant frequency analysis of EEG reveals brain's response during injury and recovery. IEEE Trans Biomed Eng 1996;43:1083–92.

Goncharova II, McFarland DJ, Vaughan TM, Wolpaw JR. EMG contamination of EEG: spectral and topographical characteristics. Clin Neurophysiol 2003;114:1580–93.

Hemmings HC, Hopkins PM. Foundations of anesthesia: basic sciences for clinical practice. 2nd ed. Philadelphia: Mosby Elsevier; 2006.

Hugelin A, Bonvallet M, Dell P. Activation recticulare et corticule d'origine chemoceptive au cours de l'hypoxie. Electroencephalography Clin Neurophysiol 1959;11:325–32.

Jung TP, Makeig S, Humphries C, Lee TW, McKeown MJ, Iragui V, et al. Removing electroencephalographic artifacts by blind source separation. Psychophysiology 2000;37:163–78.

Ma J, Bayram S, Tao P, Svetnik V. High-throughput ocular artifact reduction in multichannel electroencephalography (EEG) using component subspace projection. J Neurosci Meth 2011;196:131–40.

Makeig S, Bell AJ, Jung TP, Sejnowski TJ. Independent component analysis of electroencephalographic data. In: Advances in neural information processing systems. Cambridge, Mass: MIT Press 1996;8:145–51.

McFarland DJ, Lefkowicz AT, Wolpaw JR. Design and operation of an EEG-based brain-computer interface with digital signal processing technology. Behav Res Methods Instrum Comput 1997;29:337–45.

Pinheiro JC, Bates DM. Mixed-effects models in S and S-PLUS. New York: Springer-Verlag; 2000.

Seber GAF. Multivariate observations. New York: Wiley; 1984.

Urrestarazu E, Iriarte J, Alegre M, Valencia M, Viteri C, Artieda J. Independent component analysis removing artifacts in ictal recordings. Epilepsia 2004;45:1071–8.